CHEMISTRY OF MATERIALS

Caltech Library

Subscriber access provided by Caltech Library

Article

Reduction of aqueous CO2 to 1-Propanol at MoS2 electrodes

Sonja A. Francis, Jesus M. Velazquez, Ivonne M. Ferrer, Daniel A. Torelli, Dan Guevarra, Matthew T. McDowell, Ke Sun, Xinghao Zhou, Fadl H. Saadi, Jimmy John, Matthias H. Richter, Forrest P. Hyler, Kimberly M. Papadantonakis, Bruce S. Brunschwig, and Nathan S. Lewis

Chem. Mater., **Just Accepted Manuscript** • DOI: 10.1021/acs.chemmater.7b04428 • Publication Date (Web): 13 Jun 2018

Downloaded from http://pubs.acs.org on June 13, 2018

Just Accepted

"Just Accepted" manuscripts have been peer-reviewed and accepted for publication. They are posted online prior to technical editing, formatting for publication and author proofing. The American Chemical Society provides "Just Accepted" as a service to the research community to expedite the dissemination of scientific material as soon as possible after acceptance. "Just Accepted" manuscripts appear in full in PDF format accompanied by an HTML abstract. "Just Accepted" manuscripts have been fully peer reviewed, but should not be considered the official version of record. They are citable by the Digital Object Identifier (DOI®). "Just Accepted" is an optional service offered to authors. Therefore, the "Just Accepted" Web site may not include all articles that will be published in the journal. After a manuscript is technically edited and formatted, it will be removed from the "Just Accepted" Web site and published as an ASAP article. Note that technical editing may introduce minor changes to the manuscript text and/or graphics which could affect content, and all legal disclaimers and ethical guidelines that apply to the journal pertain. ACS cannot be held responsible for errors or consequences arising from the use of information contained in these "Just Accepted" manuscripts.

ACS Publications

is published by the American Chemical Society. 1155 Sixteenth Street N.W., Washington, DC 20036

Published by American Chemical Society. Copyright © American Chemical Society. However, no copyright claim is made to original U.S. Government works, or works produced by employees of any Commonwealth realm Crown government in the course of their duties.

Reduction of aqueous CO_2 to 1-Propanol at MoS_2 electrodes

Sonja A. Francis[†,a, 1], Jesus M. Velazquez[†a, 2], Ivonne M. Ferrer[a,], Daniel A. Torelli[a], Dan Guevarra[a], Matthew T. McDowell[a, 3], Ke Sun[a], Xinghao Zhou[b], Fadl H. Saadi[b], Jimmy John[a], Matthias H. Richter[a], Forrest P. Hyler[c], Kimberly M. Papadantonakis[a], Bruce S. Brunschwig[d], Nathan S. Lewis*[,a,d]

[a]Division of Chemistry and Chemical Engineering, [b]Division of Engineering and Applied Sciences, [c]University of California, Davis, California 95616, [d]Beckman Institute, California Institute of Technology, Pasadena, California 91125

ABSTRACT: Reduction of carbon dioxide in aqueous electrolytes at single-crystal MoS_2 or thin-film MoS_2 electrodes yields 1-propanol as the major CO_2 reduction product, along with hydrogen from water reduction as the predominant reduction process. Lower levels of formate, ethylene glycol, and t-butanol were also produced. At an applied potential of -0.59 V versus a reversible hydrogen electrode, the Faradaic efficiencies for reduction of CO_2 to 1-propanol were ~3.5% for MoS_2 single crystals and ~1% for thin films with low edge-site densities. Reduction of CO_2 to 1-propanol is a kinetically challenging reaction that requires the overall transfer of 18 e^- and 18 H^+ in a process that involves the formation of 2 C-C bonds. NMR analyses using $^{13}CO_2$ showed the production of ^{13}C-labelled 1-propanol. In all cases, the vast majority of the Faradaic current resulted in hydrogen evolution via water reduction. H_2S was detected qualitatively when single-crystal MoS_2 electrodes were used, indicating that some desulfidization of single crystals occurred under these conditions.

Introduction

The selective production of liquid carbon-containing products at low absolute overpotentials is a desirable attribute of electrocatalytic CO_2 reduction processes. Efficient catalysts operating in contact with aqueous electrolytes under ambient pressure must have minimal activity for the competing water-reduction reaction and must operate at high turnover rates under such conditions, due to the high concentration of water (~56 M) and the relatively low concentration of dissolved CO_2 (~34 mM) at 1 atm.[1] To date, few catalysts have satisfied any of these requirements, and no catalyst has met all of these criteria.[2-3]

Electrochemical CO_2 reduction (CO_2R) over transition metals such as Pd, Au, or Sn typically yields two-electron reduction products, such as carbon monoxide or formate, at moderate rates and low overpotentials, η.[4-8] Copper yields high (> 70%) Faradaic efficiencies for the production of methane and ethylene relative to other transition metals, yet Cu requires a large overpotential ($-\eta \sim 1$ V to drive a current density of -1 mA cm^{-2}) and/or exhibits low selectivity for hydrocarbons.[9-12] In some cases Cu can be tuned to generate ethanol or small amounts of 1-propanol at yields between 1-15% with $-\eta > 800$ mV.[13] Electrochemical reduction of CO_2 over Ni-Ga bimetallic catalysts yields the higher-order products methane, ethane and ethylene, albeit at low Faradaic efficiencies ($\leq$ 2%).[14] Electrochemical reduction of CO_2 over the closely related Ni-Al catalysts also has been shown to yield higher-order products, namely 1-propanol and methanol, along with substantial Faradaic efficiencies (~30%) for the formation of a two-electron reduction product, carbon monoxide. [15]

Molybdenum disulfide (MoS_2) is a layered transition-metal dichalcogenide that has found use in a variety of applications owing to its distinctive electronic, optical and catalytic properties. Extensive studies have contributed to the understanding of the catalytic and optoelectronic roles of terrace, edge, and defect sites on MoS_2 and other transition metal dichalcogenides (e.g. p-WSe_2).[16-17] MoS_2 thin films have been designed with increased densities of edge sites (under-coordinated Mo and S) to yield improved electrocatalytic activity for the reduction of protons in water to H_2.[18]

Theoretical and empirical studies have suggested that transition metal dichalcogenides may constitute promising catalysts for CO_2R.[19] Theory has suggested that MoS_2 and $MoSe_2$ can break the linear thermodynamic scaling laws that govern the behavior of transition metal catalysts by allowing CO_2R intermediates to be stabilized independently on either the metal (Mo) sites or the covalent (S or Se) sites. Empirically, MoS_2 single crystals covered with MoS_2 flakes and operated in contact with ionic liquid electrolytes have been shown to convert CO_2 to CO with ~98% Faradaic efficiency at an electrode potential, *E*, of -0.764 V versus the reversible hydrogen electrode (RHE). At this potential, MoS_2 sustained a current density of -65 mA cm^{-2}, whereas Ag nanoparticles produced a current density of -110 mA cm^{-2} with only 65% selectivity for CO.[20] Bismuth-doped MoS_2 nanosheets operated in contact with a non-aqueous imidazolium ionic liquid electrolyte dissolved in CH_3CN have been reported to be active catalysts for methanol production, with Faradaic efficiencies of 71%.[16] However, isotopic labeling experiments to confirm that the methanol was derived from CO_2, and not from other sources of carbon such as the ionic liquid itself, epoxy, or other carbon compounds used to construct the cell, have not yet been reported.[10] Interestingly, the catalytic performance in ionic liquids by MoS_2 in the conversion of CO_2R to CO improves substantially when vertically aligned MoS_2 is doped with 5% niobium.[21] Furthermore, metallic Mo, as well as Mo oxide, are active for the reduction of CO_2 to methanol and CO, respectively.[22]

We report herein on the activity of single crystals and thin films of MoS_2 for the reduction of CO_2 dissolved in an aqueous electrolyte.

Experimental section

Chemicals and materials

Sodium carbonate (Sigma Aldrich, ≥99.999%), potassium phosphate dibasic and potassium phosphate monobasic (Fisher Scientific), carbon dioxide (AirGas, Alphagaz 1), nitrogen (AirGas, Alphagaz 1), and Selemion anion-exchange membrane were used as received, unless noted otherwise. Water with a resistivity > 18 MΩ cm was obtained from a Barnsted Nanopure system.

Sample preparation

Large MoS_2 single crystals were purchased from 2D Semiconductors. These crystals were mechanically exfoliated with Scotch tape, masked with electroplating tape (3M^{TM} Electroplating tape 470) to expose large terraces, and before use were gently dried with a stream of N_2(g).

MoS_2 thin films were prepared on 525 µm-thick, HF-etched, degeneratively doped polished Si wafers (Addison Engineering, Prime grade, (100)-oriented, As-doped, resistivity <0.005 Ω cm). Mo precursor was deposited at room temperature via reactive RF sputtering from a metallic Mo target using an AJA high-vacuum magnetron sputtering system (AJA International Inc.). The Ar flow was 17 sccm, the working pressure was 5 mTorr, the sputtering power was 150 W. The sputtering time was either 30 s or 300 s. The sputtered Mo precursor films were annealed in a custom-built vacuum tube furnace (PVI) ramped at 15 °C min^{-1} to 500 °C, held for 1 h, then cooled to 80 °C over a 3 h period. A continuous flow of 10% H_2S at 400 torr in N_2(g) was maintained at each step. The total flow rate was 120 sccm through a cross-sectional diameter of 11.4 cm.

Sample characterization

High-resolution transmission electron microscopy (HRTEM) was performed on polycrystalline MoS_2 thin films that were grown directly onto thin (~50 nm) Si_xN window TEM grids with window sizes of ~500 µm x ~500 µm. Mo precursor was sputtered directly onto these grids and was then sulfurized as described previously. Plan-view (i.e., through-film) HRTEM images of the MoS_2 thin films were collected using a Tecnai F30ST TEM (FEI, Hillsboro, OR) operating at an accelerating voltage of 300 kV.

X-ray photoelectron spectroscopy (XPS) was performed using an AXIS Ultra DLD instrument (Kratos Analytical) with a background pressure of 1×10^{-9} Torr. High-intensity excitation was provided by monochromatic Al Kα X-rays having an energy of 1486.6 eV with an instrumental resolution of 0.2 eV full width at half-maximum. Photoelectrons were collected at 0° from the surface normal at a retarding (pass) energy of 80 eV for the survey scans, whereas a pass energy of 20 eV was used for the high-resolution scans. The peak energies were calibrated against the binding energy, BE, of the adventitious C 1s peak. For quantitative analysis, the XPS signals were fitted using Casa XPS software (CASA Ltd., Teignmouth, United Kingdom) to symmetric Voigt line shapes that were composed of Gaussian (70%) and Lorentzian (30%) functions that employed a Shirley background.

Scanning tunneling microscopy was performed using an Omicron Ultra-High-Vacuum Low-Temperature Scanning Tunneling Microscope (UHV LT-STM) with a base pressure of $5x10^{-10}$ Torr. Tunneling tips were prepared by electrochemically etching a 0.25 mm diameter Tungsten wire (anode) in 3 M NaOH electrolyte. Suitable STM tips were preselected using an FEI SEM and then mounted on a Au STM tip holder. Further STM tip cleaning was performed in vacuo using a flash annealing system. MoS_2 single crystal flakes were contacted and fixed on an Omicron Mo sample plate using low outgassing Ag epoxy (EPO-TEK H20E). A fresh MoS_2 surface was prepared by exfoliation of the top layer in the sample load lock directly before pump down of the sample. The STM was cooled using liquid Nitrogen (LN_2). The STM tip and sample were mounted on the STM scanner after reaching a stable temperature of 78 K, to prevent adsorption of residual gas on the sample and tip during the cool-down process.

Electrochemistry

Electrochemical experiments were performed using BioLogic SP-200 potentiostats (Biologic, Grenoble, France) controlled by standard EC-Lab software. The uncompensated cell resistance was determined from a single-point high-frequency impedance measurement and was 85% compensated by the built-in positive-feedback software.

A sealable two-compartment H-cell (**Figure S14**) was used for the electrochemical measurements. The working electrode compartment consisted of a 40 mL Pyrex weighing bottle (Sigma) that was modified with ground glass joints (2 x 14/20 and 1 x 10/18) in the lid for holding electrodes or seals, as well as a #15 o-ring joint in the base that connected to a complementary joint in the 15-mL counter electrode compartment. The two compartments were separated by a Selemion anion-exchange membrane. The lid was removable to accommodate the large (up to 2 to 3 cm^2) working electrodes. The working electrodes were either single crystals or thin films of MoS_2. A stainless steel alligator clip was used to make electrical contact to the electrodes. A Pt gauze provided the counter electrode and Ag/AgCl (1.0 M KCl) was the reference electrode (CH instruments). The potentials, E, were converted to values relative to a reversible hydrogen electrode (RHE) as follows:

$$E \text{ vs. RHE} = E \text{ vs. Ag/AgCl} + 0.235 \text{ V} + (0.0591 \text{ V} \times \text{pH})$$
$$= E \text{ vs. Ag/AgCl} + 0.637 \text{ V}$$

Cyclic voltammetry was performed on pristine electrodes in N_2(g)-purged potassium phosphate buffer (pH 6.8). Bulk electrolysis was performed in N_2(g)-purged 0.10 M potassium phosphate buffer or 0.10 M sodium carbonate that was acidified to pH 6.8 with 1 atm CO_2. Phosphate buffer was used whenever appropriate to avoid CO_2 production from the equilibrium between HCO_3^- and CO_2. The use of phosphate buffer thus creates a "carbon-free" buffer system at comparable pH values to those used for CO_2 reduction. Na_2CO_3 was used rather than K_2CO_3 due to the substantially higher purity available for Na_2CO_3. Bulk electrolyses were performed at potentials ranging from -1.2 to -1.8 V vs. Ag/AgCl (1.0 M KCl) with a typical total charge passed of 30 to 60 C. Solutions were stirred at ~1000 rpm.

For labelling experiments, 0.10 M potassium phosphate buffer was purged with $^{13}CO_2$ (Sigma-Aldrich) and electrolyses were performed as above. For electrolyses of intermediates, 0.10 M potassium phosphate buffer at pH 6.8 was also used to closely match the pH during CO_2R in bicarbonate buffer. CO(g) and CH_4(g) (Air Liquide, 99%) at 1 atm were used for studies of reaction intermediates, and produced an approximate reactant concentration of ~1 mM according to Henry's law. In contrast, the CO_2 concentration was ~34 mM in aqueous solution.

Product analysis

An Agilent 7890 gas chromatograph (GC) equipped with HayeSepQ and Molesieve 5A columns coupled to a thermal conductivity detector (TCD) with N_2(g) (Alphagaz 1) carrier gas was used to separate and quantify H_2(g). The total run time was 14 min comprising a 9 min hold at 50 °C and a ramp to 80 °C at a rate of 8 °C min^{-1} with 6 mL of gas injected per sample. An

Agilent 7820A GC coupled with a 5977E mass spectrometer (MS) with a heated quadrupole detector and a capillary Carbon-PLOT column was used for identification and quantification of CH_4(g). The oven was set to 35 °C for 6.6 min and then ramped at 20 °C min^{-1} to 150 °C, with the temperature then maintained for 2 min. Helium (Alphagaz 1) was used as the carrier gas and 100 µL of gas was injected per sample.

A Hewlett-Packard (HP) 5890 Series II GC with a split/splitless injector, a Rtx-VRX 60 m x 0.320 mm ID x 1.8 µm column (Restek, Bellafonte, PA, USA) and a flame-ionization detector (FID) coupled to an HP 7694 Headspace autosampler was used to quantify methanol, ethanol, 1-propanol, 2-propanol, and t-butanol in the electrolyte. The injection was performed using the splitless mode for 30 s from the headspace-autosampler transfer line. The GC injector was set at 200 °C. The headspace autosampler was equipped with an oven to heat up the sample vials, an injection loop and a transfer line to the GC-FID. The autosampler oven was set to 80 °C, the injection loop was set to 90 °C and transfer line to 100 °C. All other autosampler parameters were set according to factory default parameters. The post injection split flow was 20 mL min^{-1} and the column was operated at a constant flow rate of 35 cm s^{-1} average linear velocity. The GC oven-temperature profile consisted of an initial temperature 35 °C for 6 min, an increase to 60 °C at 10 °C min^{-1} with no hold time, and an increase to 200 °C at 30 °C min^{-1} with no hold time. The GC-FID analysis run time was 24 min. The FID temperature was 225 °C. Ultra-high purity He(g) was used as the carrier gas. 5 mL of liquid after electrolysis was transferred into the GC 10-mL headspace vials. For GC-HS analysis, a liquid aliquot from the cell after electrolysis was transferred into a 20 mm headspace-sealed GC vial. Using an HP headspace autosampler, the sample vial was heated to 80 °C and agitated to promote emission of volatiles into the headspace of the sealed vial. The headspace of the vial was then analyzed by GC-FID for identification and quantification of the volatiles present in the liquid.

^{1}H NMR spectroscopy was performed on a Bruker 400 MHz spectrometer. 0.1 µL of the internal standard N,N-dimethyl formamide (DMF, Mallinckrodt Chemicals, ACS grade) was added to 2 mL of the electrolyte liquid, and 0.5 mL of this mixture was transferred into an NMR tube that contained 200 µL of D_2O. The solution was mixed well prior to analysis. A presaturation method was used to suppress the signal of water in the electrolyte and to allow visualization of the analyte peaks of interest. The low power RF pulse was set to selectively saturate signals at 4.79 ppm, while 256 scans were collected where the desired resonances were excited.

For bulk electrolysis, the masked MoS_2 single-crystal working electrode was positioned in an airtight H-type cell (**Figure S14**) that contained an aqueous solution of 0.10 M Na_2CO_3 that had been acidified to pH 6.8 under 1 atm CO_2. The working and counter (Pt) electrode compartments were separated by an anion-exchange membrane (Selemion). During potentiostatic experiments at least 25 to 60 Coulombs of charge were passed at each potential. The partial current density was calculated by the product of the Faradaic efficiency and the steady state current density at the end of the bulk electrolysis, and standard deviations are shown in **Figure S6**.

Calibrations

Calibration gases, CH_4, CO, and H_2, were purchased from Air Liquide. Tank concentrations were 15, 2.5 and 5 % respectively and were balanced with N_2 or CO_2. Dilutions were prepared in a sealed 1 or 3-L round bottom flask that contained electrolyte. The sealed round bottom flasks were purged with N_2(g) or CO_2(g) for 1 h, and then known amounts of the calibration gas were injected into the flasks. The gaseous mixture was stirred for ~ 1 min and then aliquots were removed with a gas-tight syringe and injected into the GC-TCD and GC-MS.

H_2S(g) was synthesized by drop-wise addition of 1.0 M HCl (Fluka, volumetric) to an excess of technical grade FeS (Sigma-Aldrich) in a fume hood. Dilutions were performed as described above, but with Ar as the purge gas, to produce estimates of the H_2S concentration.

NMR and GC-FID standards were prepared from Sigma Aldrich HPLC grade solvents: methanol, ethanol, 1- and 2-propanol, acetone, t-butanol, ethyl acetate, tert butyl acetate, ethylene glycol. Serial dilutions of the standards were prepared in 0.10 M sodium carbonate.

Results and Discussion

Figure 1 shows optical and scanning-electron micrographs of the surfaces of the MoS_2 crystals used in this study. Although terraces dominated the surface of the MoS_2 crystals, exposed edges were also visible. To minimize the potential contribution of microscale edge sites to the catalytic activity of electrodes, each crystal was masked to expose only a region that had few microscopic edge sites (**Figure S1**).

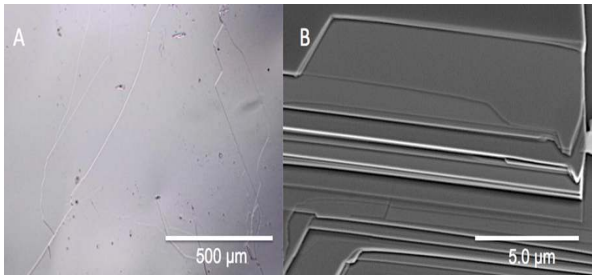

Figure 1. A) Optical micrograph of a single crystal of MoS_2. B) SEM of a region of a MoS_2 crystal showing numerous microscopic edge sites.

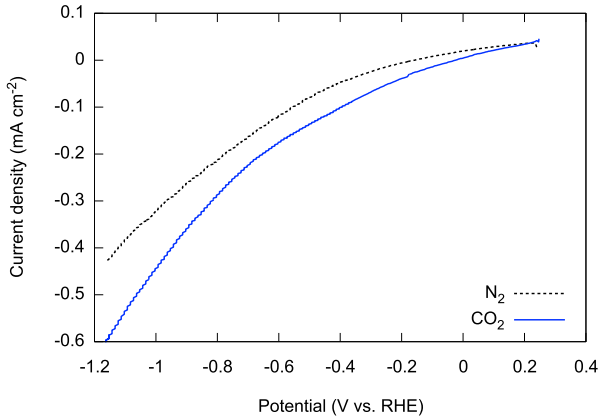

Figure 2. Comparison of linear sweep voltammograms for a MoS_2 single-crystal terrace in contact with N_2- or CO_2-purged 0.10 M K_2HPO_4 buffered to pH 6.8 with KH_2PO_4. The potential was swept from open circuit to -1.19 V vs. RHE at a scan rate of 50 mV s^{-1}.

Figure 2 compares a linear-sweep voltammogram (LSV) for a masked MoS_2 crystal operated in contact with a CO_2-saturated aqueous phosphate buffer (pH 6.8) with a LSV for the same sample operated in contact with a N_2-purged phosphate buffer

used as a control. The cathodic current density was more than 40% larger at all potentials for samples in contact with the CO_2-saturated electrolyte, indicating activity towards CO_2R in addition to the activity for H_2 evolution present in both the N_2-purged and CO_2-saturated electrolytes. For example, in the presence of 1 atm of CO_2, the potential required to drive a current density of -0.1 mA cm^{-2} was -0.53 V versus RHE, while in the N_2-purged electrolyte the potential required to drive the same current density was -0.66 V versus RHE.

Constant-potential electrolysis was performed using the MoS_2 single-crystal-terrace electrodes in contact with CO_2-saturated and N_2-purged electrolytes, respectively, and the electrolytes and headspaces were analyzed for gaseous and liquid reduction products. Gas chromatography (GC) with thermal conductivity detection (GC-TCD) and mass spectrometry (GC-MS) were used to detect products in the headspace, whereas ^1H nuclear magnetic resonance (NMR) spectroscopy was used to measure products in the electrolyte. Due to the low concentrations of some liquid products, GC Head Space (GC-HS) with flame-ionization detection (FID) was used as a complementary method for the quantification of some of the liquid-phase products. Details of the analysis methods are provided in the experimental section.

Constant-potential electrolyses at E = -0.59 V versus RHE using the MoS_2 single-crystal terrace electrodes in contact with a CO_2-saturated aqueous carbonate buffer (0.10 M Na_2CO_3 acidified to pH 6.8 with 1 atm CO_2) resulted in a mixture of CO_2R products including 1-propanol, formate, ethylene glycol, and t-butanol (**Figure S2** and **Figure S3**). H_2 was the dominant electrolysis product, as expected for reduction of protons in the aqueous electrolyte at the surface of MoS_2. The majority of CO_2R products were found in the liquid phase. At E = -0.59 V versus RHE, the major CO_2R products in terms of Faradaic efficiencies and partial current densities were 1-propanol and formate, and the minor CO_2R products were ethylene glycol and t-butanol, **Figure 3**. The only gaseous CO_2R product identified was methane, which was produced at a Faradaic efficiency of <0.01%. For the major CO_2R product 1-propanol, and for the minor products ethylene glycol and t-butanol, the partial current densities approached zero as the electrode was polarized to more negative potentials. This behavior deviates from the current vs. potential trend expected from typical Butler-Volmer kinetics, and suggests that other side reactions dominate the kinetics at more negative potentials. As the potential was made more negative, the Faradaic efficiency for formate production increased, and the yields of other CO_2R products decreased. No CO_2R products were observed at potentials positive of -0.5 V versus RHE.

The sum of the Faradaic efficiencies for the detected products of CO_2 and H_2O reduction was generally <100%. A portion of the missing Faradaic efficiency can be attributed to electrode corrosion resulting in the production of H_2S and possibly other corrosion products. H_2S was detected using a H_2S probe sensor and GC-TCD analysis (**Figure S4**). However, quantification of the H_2S produced was difficult due to the high solubility of H_2S in the aqueous electrolyte (solubility of $H_2S > 10^3 \times$ solubility of H_2).

The CO_2R activity of MoS_2 thin films with relatively low edge densities was compared to the activity of films having relatively high edge densities. **Figure 4** shows high-resolution TEM images of MoS_2 thin films prepared by sulfidization of sputtered Mo precursors. Increases in the thickness of the sputtered Mo film, with the thickness controlled by the duration of sputtering, resulted in films with increased edge densities. Thin films of MoS_2 are referred to herein based on the Mo sputtering time in seconds, for example films formed via sulfidization of Mo films sputtered for 30 s are referred to as 30-MoS_2.

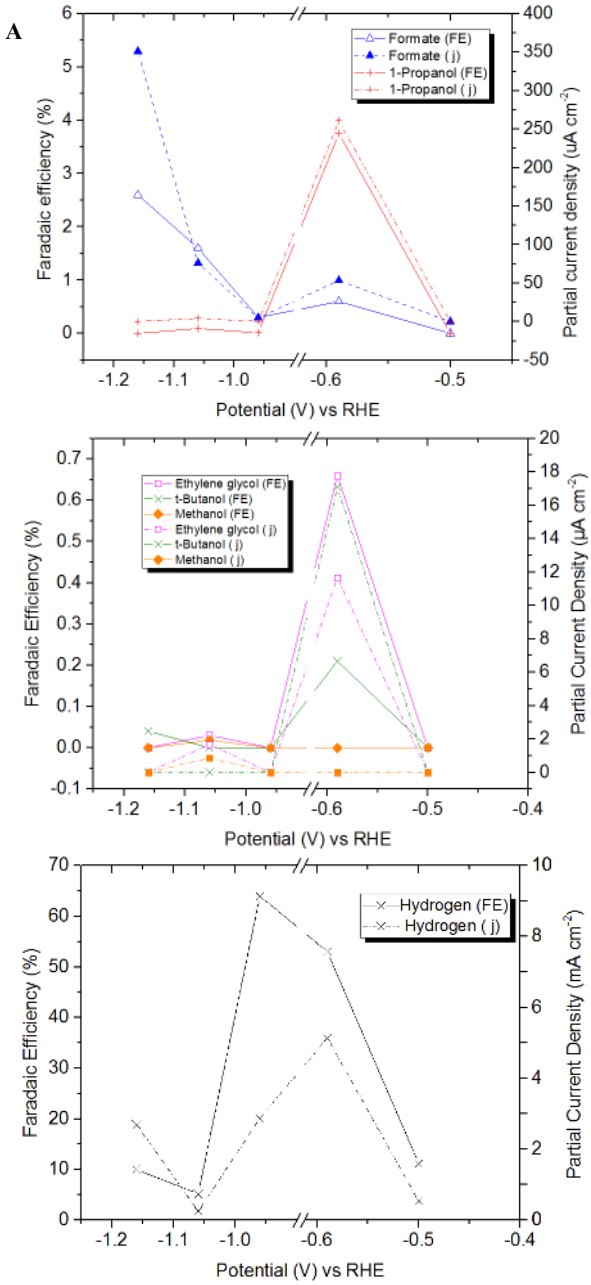

Figure 3. Potential-dependent Faradaic efficiencies (solid lines) and partial current densities (dashed lines) for major CO_2R products (A), minor CO_2R products (B), and water reduction (C) on MoS_2 single crystals with masked edge sites. The electrolyte was 0.10 M Na_2CO_3 acidified to pH 6.8 with 1 atm CO_2. The partial current density was calculated by the product of the Faradaic efficiency and the steady state current density at the end of the bulk electrolysis, and standard deviations are shown in **Figure S5**.

Figure 5 compares the Faradaic efficiencies for CO_2R products produced by constant-potential electrolyses using 30-MoS_2 electrodes and 180-MoS_2 electrodes. On 30-MoS_2, the Faradaic yields of 1-propanol reached a maximum of ~ 1% at E = -0.59 V vs. RHE and decreased at more negative potentials, whereas under the same conditions the yield of 1-propanol was ~ 0.3% for 180-MoS_2. When considered in combination with the results for MoS_2 single-crystal terrace electrodes, the increased yield of 1-propanol with a decrease in the density of edge sites suggests

that MoS_2 terraces are the active sites for reduction of CO_2 to 1-propanol. In contrast, the MoS_2 thin films produced substantially more H_2 than the single crystals, and therefore, likely less H_2S. Quantifiable yields of H_2S were not detected on the thin film electrodes.

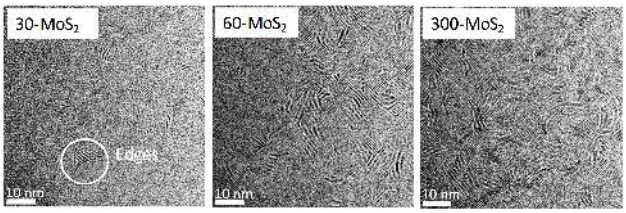

Figure 4. HRTEM images showing MoS_2 thin films prepared via various thicknesses of sputtered Mo – from left to right, 30 s, 60 s and 300 s.

Similar to the MoS_2 single-crystal terraces, the Faradaic efficiencies and partial current densities towards alcohol production on the 30-MoS_2 thin films decreased to zero or almost zero as the potential became more reducing. The possibility that the CO_2 reduction process is not electrocatalytic over MoS_2 terraces but rather is the result of a chemical reaction therefore needs to be considered. The rate of propanol production at more negative potentials was substantially lower than at -0.59 V vs. RHE. Thus the production of propanol cannot proceed by a completely chemical route. The decrease in alcohol production at more negative potentials is likely due to electrochemical side reactions becoming kinetically more important. However, the production of H_2S may suggest that electrode corrosion is part of a pathway to multicarbon products. Reduction of CO_2 to 1-propanol comprises an overall 18 H^+/e^- transfer in addition to the formation two C-C bonds.

To confirm that 1-propanol was a product of electrochemical CO_2R on MoS_2 terraces, constant-potential electrolyses at E = -0.59 V versus RHE were repeated using MoS_2 single-crystal-terrace electrodes and 30-MoS_2 thin films in contact with electrolytes saturated with $^{13}CO_2$. Under these conditions, product analyses clearly indicated the production of ^{13}C-labelled 1-propanol (**Figure 6**). The NMR analysis of the liquid products was consistent with CO_2R activity on the MoS_2 terraces. Splitting of the ^{1}H NMR spectra by ^{13}C was not clearly evident for t-butanol, ethylene glycol and formate (**Figure S8**).

To gain insight into possible mechanisms for the CO_2R process at MoS_2 single-crystal-terrace electrodes, constant-potential electrolyses were performed at E = -0.59 V versus RHE using a phosphate-buffered electrolyte (0.10 M, pH = 6.8) that was purged with either CO or CH_4. Reduction of CO yielded CH_4 as a major product, while reduction of CH_4 yielded the C_2 products ethane and ethylene (**Figures S9** and **S10**). These products were not observed in substantial quantities in the direct reduction of CO_2. These results suggest that formation of 1-propanol on MoS_2 single-crystal terraces involves the coupling of species produced during CO_2R. Furthermore, the local influence of the pH may shift the effective overpotential and lead to the formation of other species by disproportionation reactions.[23]

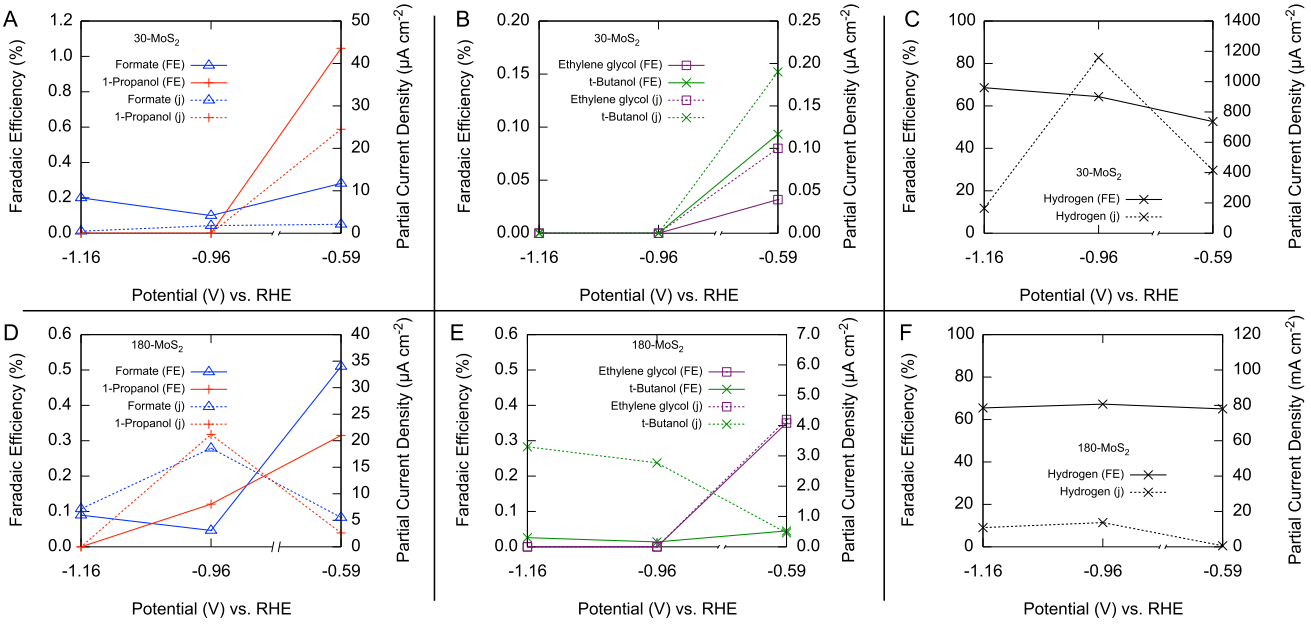

Figure 5. Potential-dependent Faradaic efficiencies (solid lines) and partial current densities (dashed lines) for major CO_2R products (A,D), minor CO_2R products (B,E), and proton reduction (C,F) on MoS_2 thin films operated in contact with 0.10 M Na_2CO_3 acidified to pH 6.8 with 1 atm CO_2. The partial current was calculated by the product of the Faradaic efficiency and the steady state current at the end of the bulk electrolysis, and standard deviations are shown in **Figure S6** and **S7**.

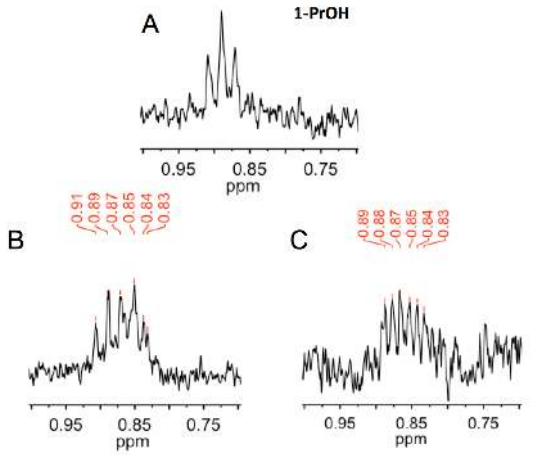

Figure 6. Representative ^{1}H NMR spectra in the 3H,t 1-propanol region showing (A) 1-propanol produced during unlabelled CO_2R on 30-MoS_2 thin films, (B) labelled 1-propanol production from $^{13}CO_2R$ 30-MoS_2 (C) labelled 1-propanol production from $^{13}CO_2R$ on MoS_2 single-crystal-terraces. Electrolyses were performed at -0.59 V vs. RHE in 0.10 M Na_2CO_3 electrolyte acidified to pH 6.8 with 1 atm of reactant gas.

The sums of the Faradaic efficiencies for formation of the reduction products were consistently and substantially below 100% for electrolysis using MoS_2 thin films or MoS_2 single-crystal-terrace electrodes. This result suggests that current was lost to other processes such as the reduction of the MoS_2 material itself, producing H_2S and a reduced metal species. The detection of H_2S suggests that the materials used herein are unstable under CO_2R conditions. Decomposition or desulfidization of MoS_2 under operating conditions may thus provide a route for the reduction of CO_2 to energy-dense hydrocarbons. X-ray photoelectron spectra collected before and after CO_2R did not show an increase in metallic Mo or Mo oxides after CO_2R (**Figure S11**). Decomposition of MoS_2 to produce H_2S and a reduced metal species is a potential-dependent reaction that can be suppressed by operating the MoS_2 electrodes at more positive potentials than those required to observe the CO_2R products herein, by reducing the concentration of protons in the electrolyte, or both.

Recent theoretical and experimental work has identified sulfur vacancies as active sites for H_2 generation, whereas desulfidization of MoS_2 monolayers occurs at more negative potentials (i.e. E = -0.6 to -1.0 V vs. RHE).[24] Theoretical studies suggest that sulfur vacancies on terraces of MoS_2 are catalytically active towards the formation of methanol via a CO hydrogenation process,[25] consistent with the presence of sulfur vacancies on MoS_2 single crystals used in this study (**Figure S12**). However, in this work reduction of CO yielded CH_4 as the major product, rather than either methanol (the product expected from theory) or 1-propanol (the major CO_2R product observed herein). Further experimental work, performed alongside theoretical studies, would be needed to elucidate the active sites and intermediates that enable CO_2 reduction to 1-propanol on MoS_2 surfaces.

Layers of MoS_2 that are weakly bonded by van der Waals forces may allow for exfoliation of a decomposed layer and exposure of a fresh surface underneath the topmost initial layer of the electrode. The stability of a MoS_2 thin film throughout a long-term electrolysis is shown in **Figure 7**. The cathodic current density rapidly decreased initially and then increases slowly, showing that the catalyst surface changes under operating conditions. Products were only detected after the electrolysis was allowed to proceed for a minimum of -20 C of charge passed or until > 10 μM products were generated, normally requiring 5–10 h). In addition, an open-circuit test was conducted with a MoS_2 electrode immersed for 16 h in CO_2-purged 0.10 M Na_2CO_2. No CO_2 reduction products were detected, and the open-circuit potential remained within ±25 mV of the initial value (+410 mV vs RHE), **Figure S13**. The absence of CO_2 reduction products from electrodes held at open circuit corroborates the suggestion that the production of alcohols is an electrochemical (potential-dependent) corrosion process.

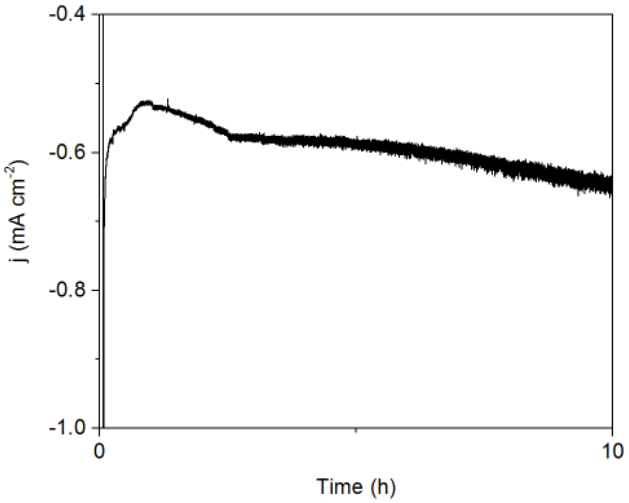

Figure 7. Long-term bulk electrolysis using 30-MoS_2 thin film at -0.59 V vs. RHE in 0.10 M Na_2CO_3 electrolyte acidified to pH 6.8 with 1 atm CO_2. The current fluctuates due to bubble formation at electrode surface.

Conclusions

Reduction of CO_2 at the surface of MoS_2 electrodes held potentiostatically at -0.59 V versus RHE while in contact with aqueous electrolytes at room temperature yielded 1-propanol as the major CO_2R product, with Faradaic efficiencies of 2-5%. Formate, t-butanol, and ethylene glycol were also produced at lower efficiencies (<1%) than for 1-propanol. The yields of 1-propanol were higher for single-crystal-terrace electrodes and for thin films with low edge-site densities than for thin films with high densities of edge sites, suggesting that the active sites for reduction of CO_2 to 1-propanol are terraces rather than edges. Qualitative evidence of H_2S evolution was observed, suggesting that the reduction of CO_2 to 1-propanol may involve desulfidization of the MoS_2. Although the reaction may not be truly catalytic, the reduction of CO_2 to a C_3 product, a reaction requiring the overall transfer of 18 protons and 18 electrons, is remarkable. An understanding of the mechanism for the reduction of CO_2 to 1-propanol at MoS_2 terraces may provide insight to guide the design of electrocatalysts capable of reducing CO_2 to fuels with greater energy densities than the C_1 products typically produced by electrochemical CO_2R.

ASSOCIATED CONTENT

Supporting Information

The Supporting Information is available free of charge on the ACS Publications website.

14 Figures, 1 Table including chromatograms, spectra and descriptions of equipment. (PDF)

AUTHOR INFORMATION

Corresponding Author

* Email: nslewis@caltech.edu.

Present Addresses

[1] Department of Chemistry, Princeton University.
[2] Department of Chemistry, University of California, Davis.
[3] G. W. Woodruff School of Mechanical Engineering and School of Materials Science and Engineering, Georgia Institute of Technology.

Author Contributions

†These authors contributed equally (S.A.F. and J.M.V.).

Funding Sources

This material is based upon work performed by the Joint Center for Artificial Photosynthesis, a DOE Energy Innovation Hub, supported through the Office of Science of the U.S. Department of Energy under Award No. DE-SC0004993. S.A.F. acknowledges the Resnick Sustainability Institute at Caltech for a Postdoctoral Fellowship. J.M.V. acknowledges support through an NRC Ford Foundation Postdoctoral Fellowship and UC Davis startup funds. D.A.T. acknowledges support through a Graduate Research Fellowship from the National Science Foundation. S.F. acknowledges the Resnick Institute at Caltech for a postdoctoral fellowship.

Notes

The authors declare no competing financial interest.

ACKNOWLEDGMENT

We thank Dr. Nathan Dalleska and Dr. David VanderVelde of the Environmental Analysis Center and High Resolution NMR Facility, respectively, for many useful discussions and instrumental access and assistance.

ABBREVIATIONS

CO_2R, carbon dioxide reduction
30-MoS_2, molybdenum disulfide thin film sulfidized for 30 seconds
180-MoS_2, molybdenum disulfide thin film sulfidized for 180 seconds.

REFERENCES

(1) Chen, Y. K.; Lewis, N. S.; Xiang, C. X., Operational constraints and strategies for systems to effect the sustainable, solar-driven reduction of atmospheric CO_2. *Energy Environ. Sci.* **2015**, 8, 3663-3674.

(2) Qiao, J.; Liu, Y.; Hong, F.; Zhang, J., A review of catalysts for the electroreduction of carbon dioxide to produce low-carbon fuels. *Chem. Soc. Rev.* **2014**, 43, 631-75.

(3) Hori, Y., Electrochemical CO2 Reduction on Metal Electrodes. In *Modern Aspects of Electrochemistry*, Vayenas, C., Ed. Springer: New York, 2008, 42, pp 89-189.

(4) Li, C. W.; Kanan, M. W., CO_2 Reduction at Low Overpotential on Cu Electrodes Resulting from the Reduction of Thick Cu_2O Films. *J. Am. Chem. Soc.* **2012**, 134, 7231-7234.

(5) Chen, Y. H.; Li, C. W.; Kanan, M. W., Aqueous CO_2 Reduction at Very Low Overpotential on Oxide-Derived Au Nanoparticles. *J. Am. Chem. Soc.* **2012**, 134, 19969-19972.

(6) Zhou, X. H.; Liu, R.; Sun, K.; Chen, Y. K.; Verlage, E.; Francis, S. A.; Lewis, N. S.; Xiang, C. X., Solar-Driven Reduction of 1 atm of CO2 to Formate at 10% Energy-Conversion Efficiency by Use of a TiO2-Protected III-V Tandem Photoanode in Conjunction with a Bipolar Membrane and a Pd/C Cathode. *ACS Energy Lett.* **2016**, 1, 764-770.

(7) Hahn, C.; Abram, D. N.; Hansen, H. A.; Hatsukade, T.; Jackson, A.; Johnson, N. C.; Hellstern, T. R.; Kuhl, K. P.; Cave, E. R.; Feaster, J. T.; Jaramillo, T. F., Synthesis of thin film AuPd alloys and their investigation for electrocatalytic CO_2 reduction. *J. Mater. Chem. A* **2015**, 3, 20185-20194.

(8) Kortlever, R.; Peters, I.; Koper, S.; Koper, M. T. M., Electrochemical CO_2 Reduction to Formic Acid at Low Overpotential and with High Faradaic Efficiency on Carbon-Supported Bimetallic Pd-Pt Nanoparticles. *ACS Catal.* **2015**, 5, 3916-3923.

(9) Kuhl, K. P.; Cave, E. R.; Abram, D. N.; Jaramillo, T. F., New insights into the electrochemical reduction of carbon dioxide on metallic copper surfaces. *Energy Environ. Sci.* **2012**, 5, 7050-7059.

(10) Hori, Y.; Kikuchi, K.; Suzuki, S., Production Of CO And CH_4 In Electrochemical Reduction Of CO_2 At Metal-Electrodes In Aqueous Hydrogencarbonate Solution. *Chem. Lett.* **1985**, 14, 1695-1698.

(11) Hori, Y.; Murata, A.; Takahashi, R., Formation Of Hydrocarbons In The Electrochemical Reduction Of Carbon-Dioxide At A Copper Electrode In Aqueous-Solution. *J. Chem. Soc., Faraday Trans.* **1989**, 85, 2309-2326.

(12) Kas, R.; Kortlever, R.; Milbrat, A.; Koper, M. T. M.; Mul, G.; Baltrusaitis, J., Electrochemical CO_2 reduction on Cu_2O-derived copper nanoparticles: controlling the catalytic selectivity of hydrocarbons. *Phys. Chem. Chem. Phys.* **2014**, 16, 12194-12201.

(13) Hori, Y.; Takahashi, I.; Koga, O.; Hoshi, N., Electrochemical reduction of carbon dioxide at various series of copper single crystal electrodes. *J. Mol. Catal. A: Chem.* **2003**, 199, 39-47.

(14) Torelli, D. A.; Francis, S. A.; Crompton, J. C.; Javier, A.; Thompson, J. R.; Brunschwig, B. S.; Soriaga, M. P.; Lewis, N. S., Nickel-Gallium-Catalyzed Electrochemical Reduction of CO_2 to Highly Reduced Products at Low Overpotentials. *ACS Catal.* **2016**, 6, 2100-2104.

(15) Paris, A. R.; Bocarsly, A. B., Ni–Al Films on Glassy Carbon Electrodes Generate an Array of Oxygenated Organics from CO_2. *ACS Catal.* **2017**, 6815-6820.

(16) Velazquez, J. M.; John, J.; Esposito, D. V.; Pieterick, A.; Pala, R.; Sun, G.; Zhou, X.; Huang, Z.; Ardo, S.; Soriaga, M. P.; Brunschwig, B. S.; Lewis, N. S., A scanning probe investigation of the role of surface motifs in the behavior of p-WSe2 photocathodes. *Energy Environ. Sci.* **2016**, 9, 164-175.

(17) Jaramillo, T. F.; Jørgensen, K. P.; Bonde, J.; Nielsen, J. H.; Horch, S.; Chorkendorff, I., Identification of Active Edge Sites for Electrochemical H_2 Evolution from MoS_2 Nanocatalysts. *Science* **2007**, 317, 100-102.

(18) Wang, H.; Lu, Z.; Xu, S.; Kong, D.; Cha, J. J.; Zheng, G.; Hsu, P.-C.; Yan, K.; Bradshaw, D.; Prinz, F. B.; Cui, Y., Electrochemical tuning of vertically aligned MoS_2 nanofilms and its application in improving hydrogen evolution reaction. *Proc. Natl. Acad. Sci. U. S. A.* **2013**, 110, 19701-19706.

(19) Chan, K.; Tsai, C.; Hansen, H. A.; Norskov, J. K., Molybdenum Sulfides and Selenides as Possible Electrocatalysts for CO_2 Reduction. *Chemcatchem* **2014**, 6, 1899-1905.

(20) Asadi, M.; Kumar, B.; Behranginia, A.; Rosen, B. A.; Baskin, A.; Repnin, N.; Pisasale, D.; Phillips, P.; Zhu, W.; Haasch, R.; Klie, R. F.; Kral, P.; Abiade, J.; Salehi-Khojin, A., Robust carbon dioxide reduction on molybdenum disulphide edges. *Nat. Commun.* **2014**, 5, 4470.

(21) Abbasi, P.; Asadi, M.; Liu, C.; Sharifi-Asl, S.; Sayahpour, B.; Behranginia, A.; Zapol, P.; Shahbazian-Yassar, R.; Curtiss, L. A.; Salehi-Khojin, A., Tailoring the Edge Structure of Molybdenum Disulfide toward Electrocatalytic Reduction of Carbon Dioxide. *ACS Nano* **2017**, 11, 453-460.

(22) Summers, D. P.; Leach, S.; Frese, K. W., The Electrochemical Reduction of Aqueous Carbon-Dioxide to Methanol at Molybdenum Electrodes with Low Overpotentials. *J. Electroanal. Chem.* **1986**, 205, 219-232.

(23) Birdja, Y. Y.; Koper, M. T. M., The Importance of Cannizzaro-Type Reactions during Electrocatalytic Reduction of Carbon Dioxide. J. Am. Chem. Soc. **2017**, 139, 2030-2034.

(24) Tsai, C.; Li, H.; Park, S.; Park, J.; Han, H. S.; Nørskov, J. K.; Zheng, X.; Abild-Pedersen, F., Electrochemical generation of sulfur vacancies in the basal plane of MoS*2* for hydrogen evolution. *Nat. Commun.* **2017**, 8, 15113.

(25) Le, D.; Rawal, T. B.; Rahman, T. S., Single-Layer MoS*2* with Sulfur Vacancies: Structure and Catalytic Application. *J. Phys. Chem. C* **2014**, 118, 5346-5351.

For table of contents only